mortality. In stark contrast, 95% of workers treated with *S. invicta* venom solution followed by formic acid solution survived (Wilcoxon: $\chi^2 = 25.4$, df = 1, $P < 0.0001$) (Fig. 3C). Thus, formic acid appears to be the compound responsible for detoxifying *S. invicta* venom.

How formic acid renders fire ant venom nontoxic is unresolved. Five principal piperidine alkaloids (2,6-dialkylpiperidines) and some of their stereoisomers primarily make up *S. invicta* venom (*10*). Suspended in this are small amounts of proteins (approximately 1% of the total), primarily the enzymes phospholipase A and hyaluronidase (*17*). The insecticidal properties of *S. invicta* venom derive directly from its alkaloids (*13*). However, associated enzymes function as cell membrane disruptors (*18*) and may be critical for gating alkaloids through intercuticular membranes and cell walls. Formic acid denatures these enzymes. This indirect effect seems the most likely detoxification mechanism. It is unknown whether formic acid alters the bioactivity of the alkaloid fraction.

N. fulva and other formicines use formic acid as a chemical weapon because it is highly caustic. Self-applying formic acid is thus costly, favoring selectivity in the expression of the detoxification behavior. We evaluated the specificity of detoxification expression by measuring its intensity after interactions with *S. invicta* versus after interactions with a series of seven test species that employ defensive compounds in interspecific conflicts. In vials, two-on-one interactions (test species versus *N. fulva*) were staged, ending when test ants applied defensive compounds to *N. fulva* (*14*). After chemical conflict with any test species, *N. fulva* workers performed significantly more detoxification behaviors than they did when there was no conflict (Fig. 4 and table S1). However, after chemical conflict with *S. invicta*, *N. fulva* workers performed the detoxification behavior with much higher frequency than after conflict with any other species (Fig. 4 and table S2). In fact, the median detoxification response after conflict with *S. invicta* was performed 6.7 times more frequently than the average response after conflicts with non–fire ant species. Curiously, detoxification behaviors were not unusually elevated after exposure to *S. richteri* workers, a closely related South American fire ant.

N. fulva and *S. invicta* share an evolutionarily ancient interaction. Although it is broadly expressed after chemical conflicts, the intense expression of detoxification behavior appears specific to interactions with *S. invicta*. We suggest that the behavior of *N. fulva* of applying toxic formic acid to its own cuticle may constitute an adaptation to competition with *S. invicta* in South America. In some South American ant assemblages, *N. fulva* is dominant to *S. invicta* but subordinate to species below *S. invicta* in the assemblage dominance hierarchy (*8*). This intransitive interaction, rare in ant assemblages, may be a hallmark, from their ancestral range, of this competitor-specific defensive adaptation.

The use of defensive compounds to achieve competitive dominance is widespread and amazingly varied in ants (*19*, *20*). Particularly potent defensive chemistries can even protect native species from extirpation by dominant invaders (*21*). However, achieving competitive dominance by self-applying a chemical as an antidote to a competitor's venom is remarkable. The ability of *N. fulva* to detoxify fire ant venom is probably a key factor contributing to the ecologically important population-level displacement of imported fire ants by *N. fulva* that is underway in areas of the southern United States (*11*).

References and Notes

1. G. J. Vermeij, *Science* **253**, 1099–1104 (1991).
2. W. F. Buren, G. E. Allen, W. H. Whitcomb, F. E. Lennartz, R. N. Williams, *J. N.Y. Entomol. Soc.* **82**, 113 (1974).
3. J. P. Pitts, thesis, University of Georgia, Athens, GA (2002).
4. A. L. Wild, *Zootaxa* **1622**, 1–55 (2007).
5. G. L. Mayr, *Verh. Zool. -Bot. Ges. Wien* **12**, 649 (1862).
6. C. Emery, *Boll. Soc. Entomol. Ital.* **37**, 107 (1906).
7. L. A. Calcaterra, F. Cuezzo, S. M. Cabrera, J. A. Briano, *Ann. Entomol. Soc. Am.* **103**, 71–83 (2010).
8. D. H. Feener Jr. *et al.*, *Ecology* **89**, 1824–1836 (2008).
9. E. G. LeBrun *et al.*, *Ecology* **88**, 63–75 (2007).
10. W. R. Tschinkel, *The Fire Ants* (Belknap Press of Harvard Univ. Press, Cambridge, MA, 2006).
11. E. G. LeBrun, J. Abbott, L. E. Gilbert, *Biol. Invas.* **15**, 2429–2442 (2013).
12. M. S. Blum, J. R. Walker, P. S. Callahan, A. F. Novak, *Science* **128**, 306–307 (1958).
13. L. Greenberg *et al.*, *Ann. Entomol. Soc. Am.* **101**, 1162–1168 (2008).
14. Methods are described in the supplementary materials.
15. J. Chen *et al.*, *Toxicon* **76**, 160–166 (2013).
16. B. D. Jackson, E. D. Morgan, *Chemoecology* **4**, 125–144 (1993).
17. M. S. Blum, *J. Toxicol. Toxin Rev.* **11**, 115–164 (1992).
18. L. D. dos Santos *et al.*, *J. Proteome Res.* **9**, 3867–3877 (2010).
19. A. N. Andersen, M. S. Blum, T. H. Jones, *Oecologia* **88**, 157–160 (1991).
20. A. Buschinger, U. Maschwitz, in *Defensive Mechanisms in Social Insects,* H. R. Hermann, Ed. (Praeger, New York, 1984), pp. 95–150.
21. T. R. Sorrells *et al.*, *PLOS ONE* **6**, e18717 (2011).

Acknowledgments: We thank M. Marischen and P. Diebold for technical assistance and N. Youssef and J. Oliver for providing *S. richteri*. E. Sarnat provided a technical drawing, and S. Stokes assisted in formulating the formic acid solution. R. Plowes provided useful discussion. Funding was provided by the Helen C. Kleberg and Robert J. Kleberg Foundation and the Lee and Ramona Bass Foundation. Data are archived at the Dryad Digital Repository, doi: 10.5061/dryad.5t110.

Supplementary Materials

www.sciencemag.org/content/343/6174/1014/suppl/DC1
Materials and Methods
Fig. S1
Tables S1 and S2
References (*22*–*33*)
Movie S1

11 September 2013; accepted 22 January 2014
10.1126/science.1245833

Resurrecting Surviving Neandertal Lineages from Modern Human Genomes

Benjamin Vernot and Joshua M. Akey*

Hybridization between closely related species, and the concomitant transfer or introgression of DNA, is widespread in nature (*1*, *2*). In hominin evolution, the sequencing of Neandertals (*3*) and their sister lineage, Denisovans (*4*, *5*), provided evidence for introgression of these lineages into modern humans. Specifically, ~1 to 3% of each non-African human genome is estimated to have been inherited from Neandertals (*3*, *5*). Although initial inferences of introgression between Neandertals and humans may not have been robust to alternative explanations—most notably, archaic population structure (*3*, *6*)—subsequent analyses have provided evidence for gene flow (*7*–*9*).

We hypothesized that a substantial amount of the Neandertal genome may be recovered from the analysis of contemporary humans despite the limited amounts of admixture, as introgressed sequences may vary among individuals (Fig. 1A). Coalescent simulations for a broad range of admixture models suggest that 35 to 70% of the Neandertal genome persists in the DNA of present-day humans (figs. S1 and S2) (*10*). By identifying Neandertal sequences from a large sample of modern humans, we hope to discover surviving

Department of Genome Sciences, University of Washington, Seattle, WA 98195, USA.

*Corresponding author. E-mail: akeyj@uw.edu

lineages that may come from multiple archaic ancestors (Fig. 1A), allowing for the recovery of population-level data.

To identify surviving Neandertal lineages, we developed a two-stage computational strategy (fig. S3) (*10*). First, we identify candidate introgressed sequences by using an extension of a previously developed summary statistic referred to as S^* (*11*), which is sensitive to the signatures of introgression (Fig. 1B) and is calculated without using the Neandertal reference genome. We performed coalescent simulations for a wide variety of demographic scenarios and found that our implementation of S^* can distinguish introgressed from nonintrogressed sequences (Fig. 1C and fig. S4). Second, we refine the set of candidate introgressed sequences using an orthogonal approach by comparing them to the Neandertal reference genome and testing whether they match significantly more than expected by chance (*10*). We estimate that the use of S^* alone, as compared to our two-staged approach, would recover ~30% of Neandertal lineages at a false discovery rate (FDR) = 20% (fig. S5) (*10*).

We applied this framework to whole-genome sequences from 379 Europeans and 286 East Asians from the 1000 Genomes Project (table S1) (*12*). Specifically, we calculated S^* in 50-kb sliding windows (tables S2 to S8) (*10*) and used a computationally efficient approach to determine statistical significance through coalescent simulations (fig. S6) (*10*). At an S^* threshold corresponding to $P \leq 0.01$, we identified ~40 Gb of candidate introgressed sequence. Note that S^* P values are robust to demographic uncertainty (fig. S7). The distribution of Neandertal-match P values for this set of candidate introgressed sequences (Fig. 1D) demonstrates a strong skew toward zero, consistent with the hypothesis that these sequences are strongly enriched for Neandertal lineages. The distribution of Neandertal-match P values for sequences that do not possess significant evidence of introgression, as revealed by S^*, is approximately uniform (Fig. 1D) (*10*), indicating that our statistical approach is able to distinguish between introgressed and nonintrogressed lineages (fig. S8) (*10*).

At FDR = 5%, we identified more than 15 Gb of introgressed sequence across all individuals, spanning ~20% (600 Mb) of the Neandertal genome (Fig. 1E and table S9). Of the 600 Mb of distinct sequence, ~25% (149 Mb) was shared between Europeans and East Asians. On average, we found 23 Mb of introgressed sequence per individual (Fig. 1F), with East Asian individuals inheriting 21% more Neandertal sequence than Europeans. Within subpopulations, we found small but statistically significant variation in the amount of introgressed sequence among Europeans (Kruskal-Wallis rank sum test, $P = 4.2 \times 10^{-12}$), but not among East Asians ($P = 0.43$).

The average length of introgressed haplotypes was ~57 kb (Fig. 2A), and ~26% of all protein-coding genes had one or more exons that overlapped a Neandertal sequence (Fig. 2B). On a broad scale, the genomic distribution of Nean-

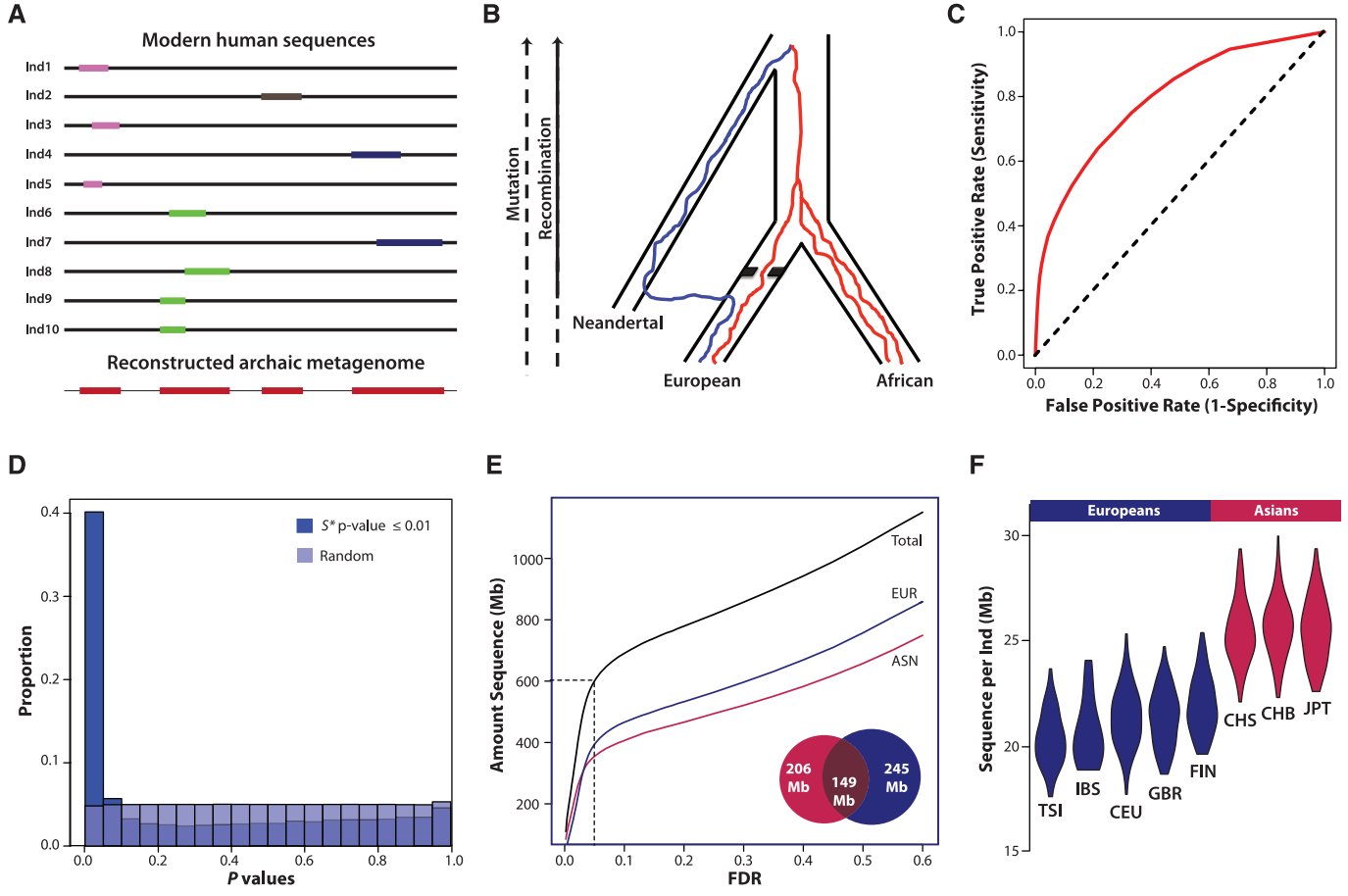

Fig. 1. Recovering Neandertal lineages from the DNA of modern humans. (**A**) Schematic representation illustrating that low levels of introgression may facilitate the recovery of substantial amounts of archaic sequence. Lines represent DNA from contemporary individuals, and colored boxes indicate archaic sequences. Different colored boxes represent sequences inherited from distinct archaic ancestors. (**B**) Genealogies of loci in Europeans and Africans in the presence of introgression. The expected signature of an introgressed lineage (blue) that our method exploits is high levels of divergence that persists over relatively long haplotype blocks. (**C**) Receiver operator curve (red) illustrating the performance of S^* for detecting an introgressed sequence in simulated data (*10*). The black diagonal dashed line represents random predictions. (**D**) Distribution of P values testing for an enrichment of Neandertal variants for S^* candidate and randomly selected regions. (**E**) Amount of Neandertal sequence recovered as a function of FDR. The inset Venn diagram shows the amount of sequence overlap between East Asians (ASN) and Europeans (EUR) at a FDR of 5%. (**F**) Violin plots showing the distribution of the amount of introgressed sequence identified per individual for East Asian and European populations (population abbreviations are described in table S1).

dertal lineages exhibits marked heterogeneity, with particular chromosomal arms, such as 8q and 17q, depleted of Neandertal sequence (Fig. 2A). These qualitative patterns were confirmed by multiple logistic regression, which showed that chromosomal arm was a significant predictor ($P < 10^{-16}$) of the odds that a 50-kb window possessed introgressed sequence (*10*) (Fig. 2C and figs. S9 and S10). Furthermore, odds ratios were negatively correlated with fixed differences between modern humans and Neandertals (Fig. 2D) (Spearman's $\rho = -0.80$, $P < 5.8 \times 10^{-8}$). A strong depletion of Neandertal lineages spanning ~17 Mb on 7q encompasses the *FOXP2* locus (Fig. 2A), a transcription factor that plays an important role in human speech and language (*13*). The observed negative correlation between odds ratio and divergence remained significant when East Asians and Europeans were analyzed separately (fig. S11) and when explicitly controlling for the presence of Neandertal lineages in modern humans (*10*) (figs. S12 and S13). These results suggest that sequence divergence between modern humans and Neandertals was a barrier to gene flow in some regions of the genome and was associated with deleterious fitness consequences (*14*).

We next leveraged the catalog of introgressed sequences in East Asians and Europeans to refine admixture models and infer parameters of gene flow between modern humans and Neandertals (figs. S14 and S15). Specifically, with the use of an approximate Bayesian computation framework (*10*), we statistically tested a model with a single pulse of introgression into the common ancestor of Europeans and East Asians (*3*), as well as a second model with gene flow both in the common ancestor and a second, smaller pulse into East Asians shortly after the two populations split (Fig. 3A). Consistent with recent inferences (*5*, *9*), observed patterns of introgression were incompatible with a one-pulse model (Fig. 3B), suggesting that gene flow between Neandertals and humans occurred multiple times. Although we varied many parameters of each model (*10*) (fig. S14), only the ratio of ancestral effective population size between Europeans and East Asians (N_e^{EUR}/N_e^{ASN}) and the relative amount of introgression between the second and first pulse (m_2/m_1) had appreciable effects on model fit (Fig. 3B). We estimate that

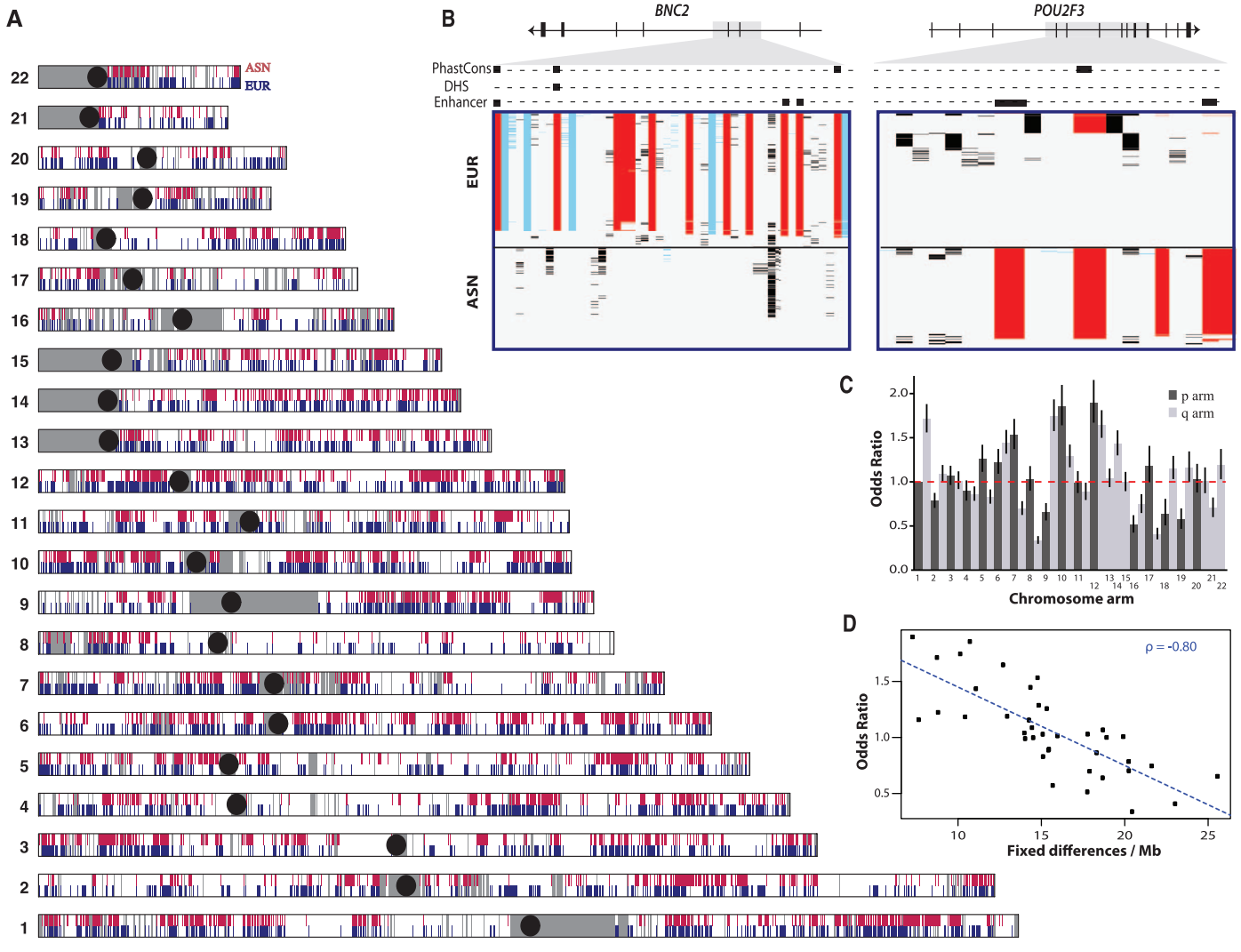

Fig. 2. Genomic distribution of surviving Neandertal lineages. (**A**) Neandertal lineages identified in East Asians (ASN, red) and Europeans (EUR, blue). Gray shading denotes regions that did not pass filtering criteria (*10*); black circles represent centromeres. (**B**) Visual genotype illustrations of introgressed sequences identified in the *BNC2* and *POU2F3* genes. Rows denote individuals, columns indicate variant sites, and rectangles are colored according to genotype (red, predicted Neandertal variant that matches the allele present in the Neandertal reference genome; blue, predicted Neandertal variant that does not match the allele present in the Neandertal reference genome; black, other variants). Introgressed variants that overlap a PhastCons conserved element, DNaseI hypersensitive site (DHS), or putative enhancer elements are shown as boxes (*10*). (**C**) Odds of finding an introgressed lineage on each chromosomal arm calculated from a logistic regression model (*10*). Odds ratios (ORs) are expressed using chromosome 1p as the baseline level. Horizontal bars represent 95% CIs. (**D**) Relation between the OR and the number of fixed differences per megabase between humans and Neandertals. ρ, Spearman's rank correlation coefficient.

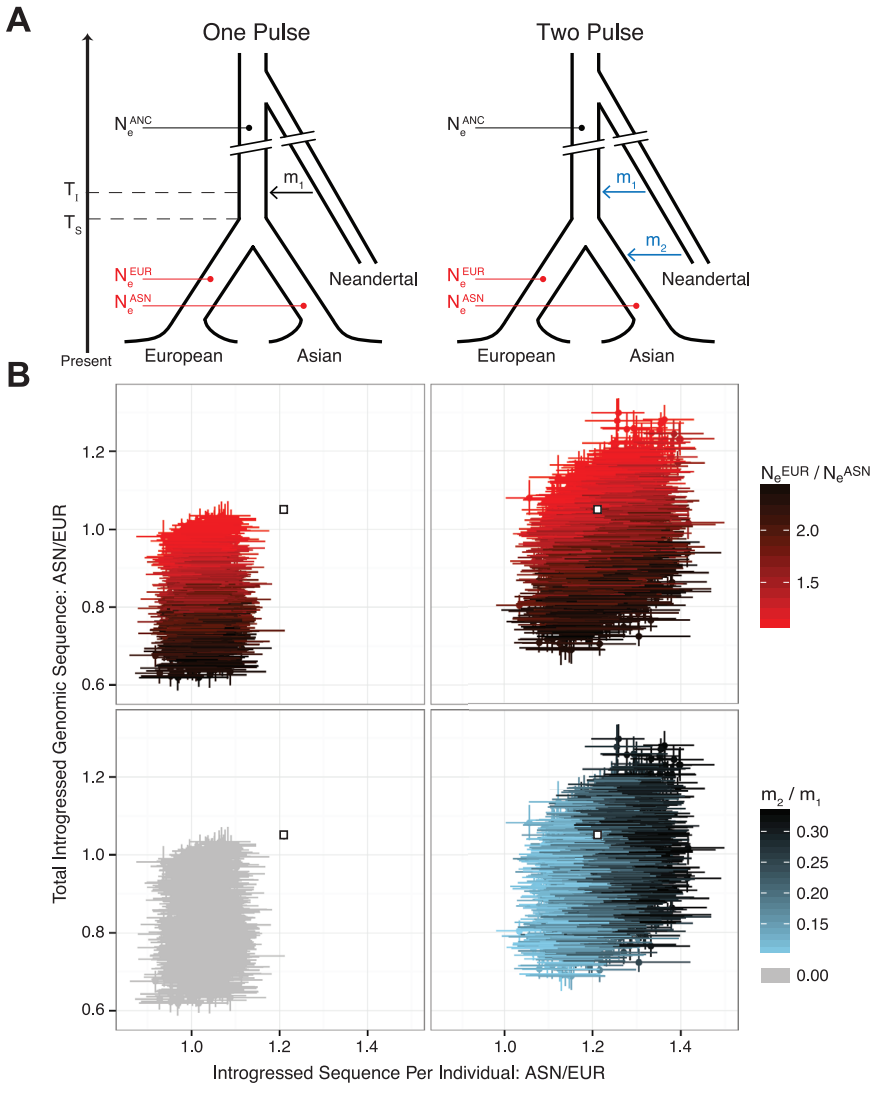

Fig. 3. Organization and characteristics of Neandertal sequence in Europeans and East Asians suggests at least two admixture events. (**A**) Schematic diagrams of the one- and two-pulse admixture models. N_e^{ANC}, N_e^{ASN}, and N_e^{EUR} denote effective population sizes of the ancestral, East Asian, and European populations, respectively. In the one-pulse model, gene flow (m_1) between Neandertals and the ancestors of Europeans and East Asians occurs at time T_I. In the two-pulse model, a second pulse of gene flow (m_2) occurs into East Asians shortly after the divergence of Europeans and East Asians at time T_S. (**B**) Values of summary statistics calculated from 2000 simulations under each model (red, blue, and grey points; horizontal and vertical bars denote 95% CIs) show that a single-pulse model is incompatible with the observed data (white box, corrected for sample size differences between populations; limits of box denote 95% CI). Simulations that varied N_e^{ASN}/N_e^{EUR} are shown in red, and those with variable m_2/m_1 are shown in blue (color bars indicate parameter values).

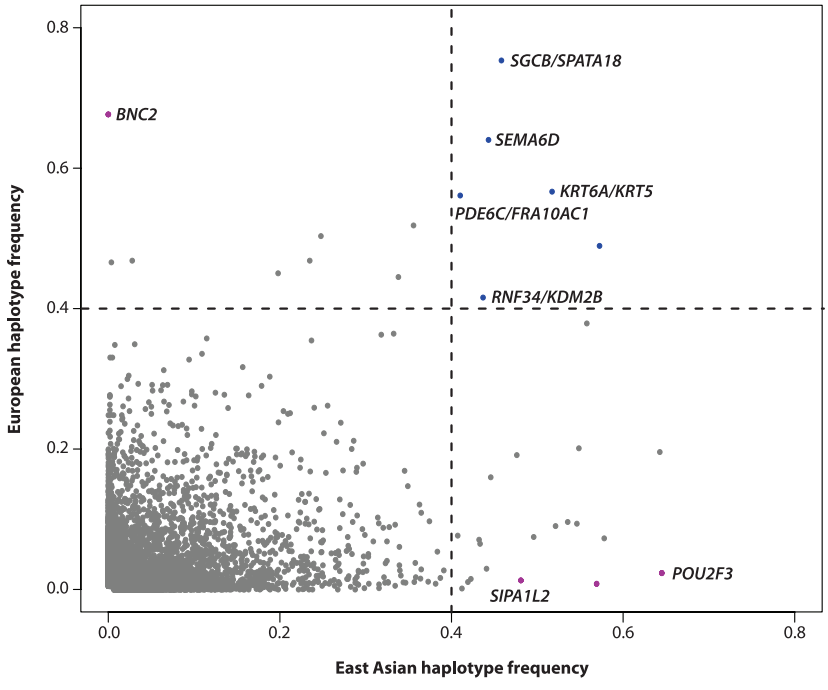

Fig. 4. Signatures of adaptive introgression. A scatter plot of introgressed haplotype frequency in Europeans and East Asians is shown. Significantly differentiated and common shared haplotypes are represented in magenta and blue, respectively. Protein-coding genes that overlap candidate adaptively introgressed loci are also shown.

N_e^{EUR}/N_e^{ASN} is 1.29 [95% confidence interval (CI) of 1.15 to 1.57] and that East Asians received 20.2% (95% CI of 13.4 to 27.1%) more Neandertal sequence in the second pulse (*10*). We note that additional unexplored models may provide a better fit to the data, and refining demographic models of hominin evolution is an important area for future work.

The collection of surviving Neandertal lineages that we identified allows us to search for signatures of adaptive introgression (*15*, *16*). First, we used introgressed variants that exhibit large allele frequency differences between Europeans and East Asians ($F_{ST} > 0.40$, $P < 0.001$ by simulation) (*10*) to identify four significantly differentiated regions (Fig. 4 and table S10) (*10*). Introgressed haplotypes in two of these regions span genes that play important roles in the integumentary system: *BNC2* on chromosome 9 and *POU2F3* on chromosome 11. *BNC2* encodes a zinc finger protein expressed in keratinocytes and other tissues (*17*) and has been associated with skin pigmentation levels in Europeans (*18*). The adaptive haplotype has a frequency of ~70% in Europeans and is completely absent in East Asians (Fig. 2B). *POU2F3* is a homeobox transcription factor expressed in the epidermis and mediates keratinocyte proliferation and differentiation (*19*, *20*). The adaptive haplotype in East Asians has a frequency of ~66% and is found at less than 1% frequency in Europeans (Fig. 2B). No coding introgressed variants were found in *BNC2* or *POU2F3*, although several highly differentiated introgressed variants were located in functional noncoding elements (*21*) (Fig. 2B), suggesting that modern humans acquired adaptive regulatory sequences at these loci. We also searched for shared signatures of adaptive introgression between East Asians and Europeans, identifying six distinct regions that have introgressed haplotype frequencies greater than 40% in both populations (Fig. 4 and table S11) ($P < 10^{-4}$ by simulation) (*10*). One of these regions lies in the type II cluster of keratin genes on 12q13 (table S11), further suggesting that Neandertals provided modern humans with adaptive variation for skin phenotypes. In total, 8 of the 10 candidate introgressed regions overlap protein-coding genes (Fig. 4).

This study shows that the fragmented remnants of the Neandertal genome carried in the DNA of modern humans can be robustly identified, allowing, in aggregate, substantial amounts of Neandertal sequence to be recovered. In principle, our approach can be used in the absence of an archaic reference sequence, potentially allowing the discovery and characterization of previously unknown hominins that interbred with modern humans (*22*–*24*). This fossil-free paradigm of sequencing archaic genomes holds considerable promise for revealing insights into hominin evolution, the population genetics characteristics of archaic hominins, how introgression has influenced extant patterns of human genomic diversity, and narrowing the search for genetic changes that endow distinctly human phenotypes.

References and Notes

1. A. D. Twyford, R. A. Ennos, *Heredity* **108**, 179–189 (2012).
2. D. Zinner, M. L. Arnold, C. Roos, *Evol. Anthropol.* **20**, 96–103 (2011).
3. R. E. Green *et al.*, *Science* **328**, 710–722 (2010).
4. D. Reich *et al.*, *Nature* **468**, 1053–1060 (2010).
5. M. Meyer *et al.*, *Science* **338**, 222–226 (2012).
6. A. Eriksson, A. Manica, *Proc. Natl. Acad. Sci. U.S.A.* **109**, 13956–13960 (2012).
7. M. A. Yang, A. S. Malaspinas, E. Y. Durand, M. Slatkin, *Mol. Biol. Evol.* **29**, 2987–2995 (2012).
8. S. Sankararaman, N. Patterson, H. Li, S. Pääbo, D. Reich, *PLOS Genet.* **8**, e1002947 (2012).
9. J. D. Wall *et al.*, *Genetics* **194**, 199–209 (2013).
10. Supplementary materials are available on *Science* Online.
11. V. Plagnol, J. D. Wall, *PLOS Genet.* **2**, e105 (2006).
12. G. R. Abecasis *et al.*, *Nature* **491**, 56–65 (2012).
13. W. Enard *et al.*, *Nature* **418**, 869–872 (2002).
14. M. Currat, L. Excoffier, *Proc. Natl. Acad. Sci. U.S.A.* **108**, 15129–15134 (2011).
15. F. L. Mendez, J. C. Watkins, M. F. Hammer, *Am. J. Hum. Genet.* **91**, 265–274 (2012).
16. L. Abi-Rached *et al.*, *Science* **334**, 89–94 (2011).
17. A. Vanhoutteghem, P. Djian, *Proc. Natl. Acad. Sci. U.S.A.* **103**, 12423–12428 (2006).
18. L. C. Jacobs *et al.*, *Hum. Genet.* **132**, 147–158 (2013).
19. A. Cabral, D. F. Fischer, W. P. Vermeij, C. Backendorf, *J. Biol. Chem.* **278**, 17792–17799 (2003).
20. H. Takemoto *et al.*, *J. Dermatol. Sci.* **60**, 203–205 (2010).
21. B. E. Bernstein *et al.*, *Nature* **489**, 57–74 (2012).
22. J. D. Wall, K. E. Lohmueller, V. Plagnol, *Mol. Biol. Evol.* **26**, 1823–1827 (2009).
23. M. F. Hammer, A. E. Woerner, F. L. Mendez, J. C. Watkins, J. D. Wall, *Proc. Natl. Acad. Sci. U.S.A.* **108**, 15123–15128 (2011).
24. J. Lachance *et al.*, *Cell* **150**, 457–469 (2012).

Acknowledgments: We thank members of the Akey laboratory, S. Browning, B. Browning, and J. Duffy for critical feedback related to this work; S. Pääbo for providing access to high-coverage Neandertal sequence data; and L. Jáuregui for help in figure preparation. A description of where sequence data used in our analyses can be found in the supplementary materials. Introgressed regions and variants can be downloaded from http://akeylab.gs.washington.edu/downloads.shtml. J.M.A. is a paid consultant of Glenview Capital.

Supplementary Materials

www.sciencemag.org/content/343/6174/1017/suppl/DC1
Materials and Methods
Figs. S1 to S15
Tables S1 to S11
References (*25*–*45*)

12 September 2013; accepted 6 December 2013
Published online 29 January 2014;
10.1126/science.1245938

Molecular Editing of Cellular Responses by the High-Affinity Receptor for IgE

Ryo Suzuki,[1] Sarah Leach,[1] Wenhua Liu,[2] Evelyn Ralston,[2] Jörg Scheffel,[1] Weiguo Zhang,[3] Clifford A. Lowell,[4] Juan Rivera[1]*

Cellular responses elicited by cell surface receptors differ according to stimulus strength. We investigated how the high-affinity receptor for immunoglobulin E (IgE) modulates the response of mast cells to a high- or low-affinity stimulus. Both high- and low-affinity stimuli elicited similar receptor phosphorylation; however, differences were observed in receptor cluster size, mobility, distribution, and the cells' effector responses. Low-affinity stimulation increased receptor association with the Src family kinase Fgr and shifted signals from the adapter LAT1 to the related adapter LAT2. LAT1-dependent calcium signals required for mast cell degranulation were dampened, but the role of LAT2 in chemokine production was enhanced, altering immune cell recruitment at the site of inflammation. These findings uncover how receptor discrimination of stimulus strength can be interpreted as distinct in vivo outcomes.

It has long been recognized that there are many subtleties in how receptors function to determine a cell's response. For example, vegetative growth of the yeast *Saccharomyces cerevisiae* is elicited by low pheromone concentrations recognized by the pheromone receptor Ste2, whereas intermediate and high pheromone concentrations sensed by this receptor lead to chemotropic growth or mating, respectively (*1*). Mathematical modeling suggests that yeast translate pheromone concentration as the duration of the transmitted signal (*2*).

We explored how the high-affinity immunoglobulin E (IgE) receptor FcεRI discriminates high- from low-affinity stimulation to modulate the mast cells' effector responses. Engagement of FcεRI on mast cells and basophils is central to allergic responses (*3*, *4*). Allergic individuals may produce IgE antibodies to offending allergens (a term used for allergy-inducing antigens). These IgE antibodies bind [via their crystallizable

[1]Laboratory of Molecular Immunogenetics, National Institute of Arthritis and Musculoskeletal and Skin Diseases, Bethesda, MD 20892, USA. [2]Light Imaging Section, Office of Science and Technology, National Institute of Arthritis and Musculoskeletal and Skin Diseases, Bethesda, MD 20892, USA. [3]Department of Immunology, Duke University School of Medicine, Durham, NC 27710, USA. [4]Department of Laboratory Medicine, University of California, San Francisco, CA 94143, USA.

*Corresponding author. E-mail: juan_rivera@nih.gov

Science
AAAS

Resurrecting Surviving Neandertal Lineages from Modern Human Genomes

Benjamin Vernot and Joshua M. Akey

Science **343**, 1017 (2014);
DOI: 10.1126/science.1245938